

Article

Fabrication of Polyethyleneimine-Modified Nanocellulose/Magnetic Bentonite Composite as a Functional Biosorbent for Efficient Removal of Cu(II)

Xiaoyin Sun ^{1,2,†}, Xintian Lv ^{1,2,†}, Caohui Han ^{1,2}, Lu Bai ^{1,2}, Tingting Wang ^{1,2} and Yongchang Sun ^{1,2,*} ¹ School of Water and Environment, Chang'an University, Xi'an 710054, China² Key Laboratory of Subsurface Hydrology and Ecological Effect in Arid Region, Ministry of Education, Chang'an University, Xi'an 710054, China

* Correspondence: ycsun@chd.edu.cn; Tel.: +86-29-82339952; Fax: +86-29-82339281

† These authors contributed equally to this work.

Abstract: A novel inorganic–organic biosorbent, polyethyleneimine (PEI)-modified nanocellulose cross-linked with magnetic bentonite, was prepared for the removal of Cu(II) from water. Fourier transform infrared spectroscopy (FT-IR) and X-ray diffraction (XRD) showed that the amino and carboxyl groups were successfully grafted onto the nanocellulose structure. The adsorption performance of Cu(II) with various factors, using the biosorbent, was investigated. The results show that the adsorption equilibrium could be reached within a short time (10 min), and the adsorption capacity of Cu(II) reached up to 757.45 mg/g. The adsorption kinetics and adsorption isotherms were well-fitted with the pseudo-second-order and the Freundlich isotherm models, respectively. The adsorption process of the composite is mainly controlled by chemisorption, and functional group chelation and electrostatic force were the adsorption mechanisms; pore filling also has a great influence on the adsorption of Cu(II). It was found that the prepared modified nanocellulose composite has great potential for the removal of heavy metals from water.

Keywords: nanocellulose; bentonite; magnetic; heavy metals; water

Citation: Sun, X.; Lv, X.; Han, C.; Bai, L.; Wang, T.; Sun, Y. Fabrication of Polyethyleneimine-Modified Nanocellulose/Magnetic Bentonite Composite as a Functional Biosorbent for Efficient Removal of Cu(II). *Water* **2022**, *14*, 2656. <https://doi.org/10.3390/w14172656>

Academic Editor: Laura Bulgariu

Received: 10 July 2022

Accepted: 25 August 2022

Published: 28 August 2022

Publisher's Note: MDPI stays neutral with regard to jurisdictional claims in published maps and institutional affiliations.



Copyright: © 2022 by the authors. Licensee MDPI, Basel, Switzerland. This article is an open access article distributed under the terms and conditions of the Creative Commons Attribution (CC BY) license (<https://creativecommons.org/licenses/by/4.0/>).

1. Introduction

With the rapid development of industrialization and urbanization, heavy metal pollution in water bodies has become more and more serious [1]. The removal methods of heavy metals from water mainly include chemical precipitation [2], ion exchange methods [3,4], and membrane filtration, etc. [4,5]. However, these methods often produce secondary contamination, and always come with high treatment costs. Adsorption has been widely used for the treatment of wastewater containing heavy metals due to its simplicity and lower costs. Recently, biobased adsorbents have attracted the researcher's attention in many studies because of its wide availability, renewability, sustainability, and the possibility of modification [6], such as biomass-derived adsorbents [7,8].

Biosorbents are naturally occurring adsorbents with superior properties over other adsorption materials; among them, cellulose is one of the most important and abundant green biomass-derived adsorbent. Cellulose, a linear biopolymer, is composed of glucose structural units linked by 1–4 glycosidic bonds, and is the most widely used and renewable biopolymer in nature, making it a very promising raw material for the preparation of various functional materials at low cost [9,10]. However, the adsorption capacity and selectivity for heavy metal ions of natural cellulose is low [8,11,12]. In recent years, the emergence of nanocellulose has greatly contributed to the development of cellulose materials. Among them, cellulose nanofibers (CNFs) formed by the 2,2,6,6-tetramethylpiperidine-1-oxyl (TEMPO) oxidation method exhibited large specific surface areas, high crystallinity, uniform widths, and high aspect ratios [13]. This oxidation process only occurs on the

surface of cellulose, and oxidizes the primary alcohol hydroxyl group to the carboxyl functional group. Since the generated carboxyl group is negatively charged, electrostatic repulsion has been observed between the cellulose surface, thus continuously promoting the cleavage of the cellulose fibers [13]. Because the crystallization area inside the cellulose fiber has low reactivity, the oxidation of cellulose fibers to finally obtain the high purity of cellulose nanocrystals is necessary for cellulose utilization [14–16]. In addition, the structure of modified CNFs is rich in sodium carboxylate anions that can interact with cationic metal ions through electrostatic interactions, as well as hydroxyl groups that can strongly interact with inorganic particles through strong van der Waals interactions. Therefore, TEMPO-oxidized cellulose nanoparticles (TOCN) were used as raw biosorbent in this study.

Currently, magnetic adsorbents have emerged as novel adsorbent materials that can achieve separation from aqueous solution through magnetism. However, magnetite nanoparticles usually coalesce in aqueous solutions, resulting in the inhibition of adsorption. Therefore, researchers have immobilized magnetite on solid carriers, such as bentonite, biochar, and organic polymer materials, which can minimize the coagulation of magnetic nanoparticles. Bentonite, as an inorganic carrier, is mainly composed of montmorillonite, a clay mineral with a negatively charged surface and a 2:1 type of aluminosilicate [17,18]. To reuse the adsorbent in a facile manner and enhance the adsorption capacity of heavy metals from water, a magnetic bentonite inorganic–organic material was successfully prepared by the co-precipitation method, and organic cellulose nanoparticles, TOCNs, were introduced into the novel composite production process.

In order to enhance the interaction between the novel cellulose composite and the heavy metals, the cellulose nanoparticles can be modified with some organic ligands or functional polymeric compounds [19]. Polyethyleneimine (PEI) is a promising adsorbent material with high densities of amines and amides, and has a strong ability to adsorb heavy metals [20,21]. Qin et al. [22] investigated the adsorption of Cu(II) using carboxymethylated CNFs (CMCNFs) containing high levels of carboxylic acid, and found that the equilibrium adsorption capacity of Cu(II) reached 115.3 mg/g at pH 5.0. Jin et al. [23] prepared a PEI-bacterial cellulose (PEI-BC) biosorbent that could achieve a maximum adsorption of Cu(II) of 148.0 mg/g. Results showed that the nanoporous architecture of BC makes it easy to adsorb Cu(II) after PEI modification. Hoang et al. [24] used the property of polyethyleneimine (PEI) with positively charged amino groups to establish interfacial polymerization with melamine (TMC), and added cellulose nanoparticles (CNCs) to prepare thin-film nanocomposite nanofiltration membranes to achieve a high removal efficiency of toxic heavy metal ions (CuSO₄ 98.0%, CuCl₂ 96.5%, PbCl₂ 90.8%). Hong et al., investigated the effects of the cellulose source and type on platinum (Pt) adsorption by PEI-modified nanocellulose. Results showed that cellulose nanofibrils from tunicates exhibited the highest PEI grafting density, and pure cellulose with an open porous structure could enhance the PEI density [25]. Therefore, nanocellulose can be grafted with PEI and cross-linked with magnetic bentonite to synthesize novel organic–inorganic composites for the efficient removal of heavy metals from water.

In this study, pure cellulose was oxidized to form nanocellulose via TEMPO, and subsequently cross-linked with PEI containing high-density amino groups using glutaraldehyde to form TOCN–PEI composites. The bentonite was also endowed with magnetic properties by co-precipitation. The magnetic bentonite and PEI-cross-linked nanocellulose were cross-linked by glutaraldehyde to prepare polyethyleneimine-modified nanocellulose/magnetic bentonite composite (PNMBC). Finally, the structure and physicochemical properties of the prepared composites were characterized by Fourier transform infrared spectroscopy (FT-IR), X-ray diffraction (XRD), Brunauer–Emmett–Teller (BET), and thermogravimetric analysis (TGA). In order to determine the Cu(II) adsorption efficiency and mechanism of PNMBC, the adsorption capacity of Cu(II) was systematically investigated by changing the pH value of the solution, adsorption time, concentration of Cu(II), and adsorption temperature.

2. Experimental

2.1. Materials

The compound 2,2,6,6-tetramethylpiperidine-1-oxyl (TEMPO) was purchased from Yuanye Biotechnology Co., Ltd. (Shanghai, China). NaBr was obtained from Fuchen Chemical Reagent Co., Ltd. (Xi'an, China), and NaClO was obtained from Fuyu Fine Chemical Co., Ltd. (Tianjin, China). NaOH, methanol, glutaraldehyde (25%), and polyethyleneimine 50% aqueous solution were purchased from Sinopharm Chemical Reagent Co., Ltd. (Tianjin, China). The anhydrous copper sulfate was used to prepare different concentrations of copper solutions, and was purchased from Tianli Chemical Reagent Co., Ltd. (Tianjin, China). Whatman double circle qualitative filter papers (medium speed) were obtained from General Electric Biotechnology Co., Ltd. (Hangzhou, China). All chemicals used were analytical grade and without any further purification.

2.2. Synthesis of TOCN

The TEMPO-oxidized cellulose nanoparticles (TOCN) were formed by the oxidation process of the filter paper fiber [14,26]. In a typical preparation process, the filter paper was dissolved and stirred in the distilled water to form a homogeneous cellulose pulp, and then the cellulose pulp was filtered to obtain the cellulose fiber. The frozen sample was freeze dried to obtain the pure cellulose fiber. Subsequently, 5 g of cellulose fiber was dispersed in 375 mL of distilled water containing TEMPO (0.0125 g) and NaBr (0.125 g), and the mixture was stirred for 15 min to ensure complete dispersion of all substances. Following this, a certain amount of NaClO was added dropwise to the slurry to oxidize the hydroxymethyl to carboxyl group [27]. After the addition of NaClO, the pH was maintained at 10 by adding 0.5 mol/L NaOH and continued stirring at 500 rpm at room temperature until there was no pH change. The reaction was terminated with 5 mL of anhydrous ethanol. The mixture was then transferred to a beaker for precipitation, and the supernatant was removed. The remaining mixture was centrifuged at 8000 rpm, and subsequently filtered and washed with distilled water and stored at room temperature.

2.3. Synthesis of TOCN-PEI

PEI was grafted onto TOCN via the glutaraldehyde cross-linking method to form the TOCN-PEI fraction [28]. The TOCN suspension was obtained by dispersing 2 g of TOCN in 100 mL methanol, and then 5 g of PEI was added to the TOCN suspension and stirred thoroughly for 24 h. The precipitate was centrifuged at 8000 rpm (to remove the residual PEI) and then added to 100 mL of deionized water, and 4 mL of 25% glutaraldehyde solution was added dropwise. The pH of the solution was adjusted to 8 with 0.4 mol/L of NaOH. The mixed solution was stirred for 1 h to cross-link the nanocellulose with PEI. Finally, the product was thoroughly separated and cleaned with deionized water and freeze dried to obtain the TOCN-PEI biosorbent.

2.4. Synthesis of Magnetic Bentonite

A mixture of 21.6240 g $\text{FeCl}_3 \cdot 6\text{H}_2\text{O}$ and 7.9524 g $\text{FeCl}_2 \cdot 4\text{H}_2\text{O}$ in water (150 mL) was poured into a well-dispersed bentonite slurry (10 g bentonite in 500 mL deionized water), then the mixture was heated to 70 °C. The pH of the mixture was adjusted to 10 by adding NaOH solution (40 mg/L) dropwise, and stirred for 4 h. Subsequently, the magnetic bentonite (MB) was separated by centrifugation and freeze dried for subsequent experiment.

2.5. Synthesis of PNMBC

The polyethyleneimine-modified nanocellulose/magnetic bentonite composite (PN-MBC) was prepared according to the scheme in Figure 1. About 0.5 g of TOCN-PEI was dissolved in 25 mL of distilled water, and 0.5 g of magnetic bentonite was dissolved in 25 mL of distilled water. These two solutions were mixed in the mass ratio of 1:1, 1:2, 2:1, respectively, and 3 mL of glutaraldehyde was added as the cross-linking agent [29]. The

mixed solution was stirred in a magnetic stirrer for about 30 min, and the stirred solution was poured into a beaker and freeze dried to produce the PNMBC sample.

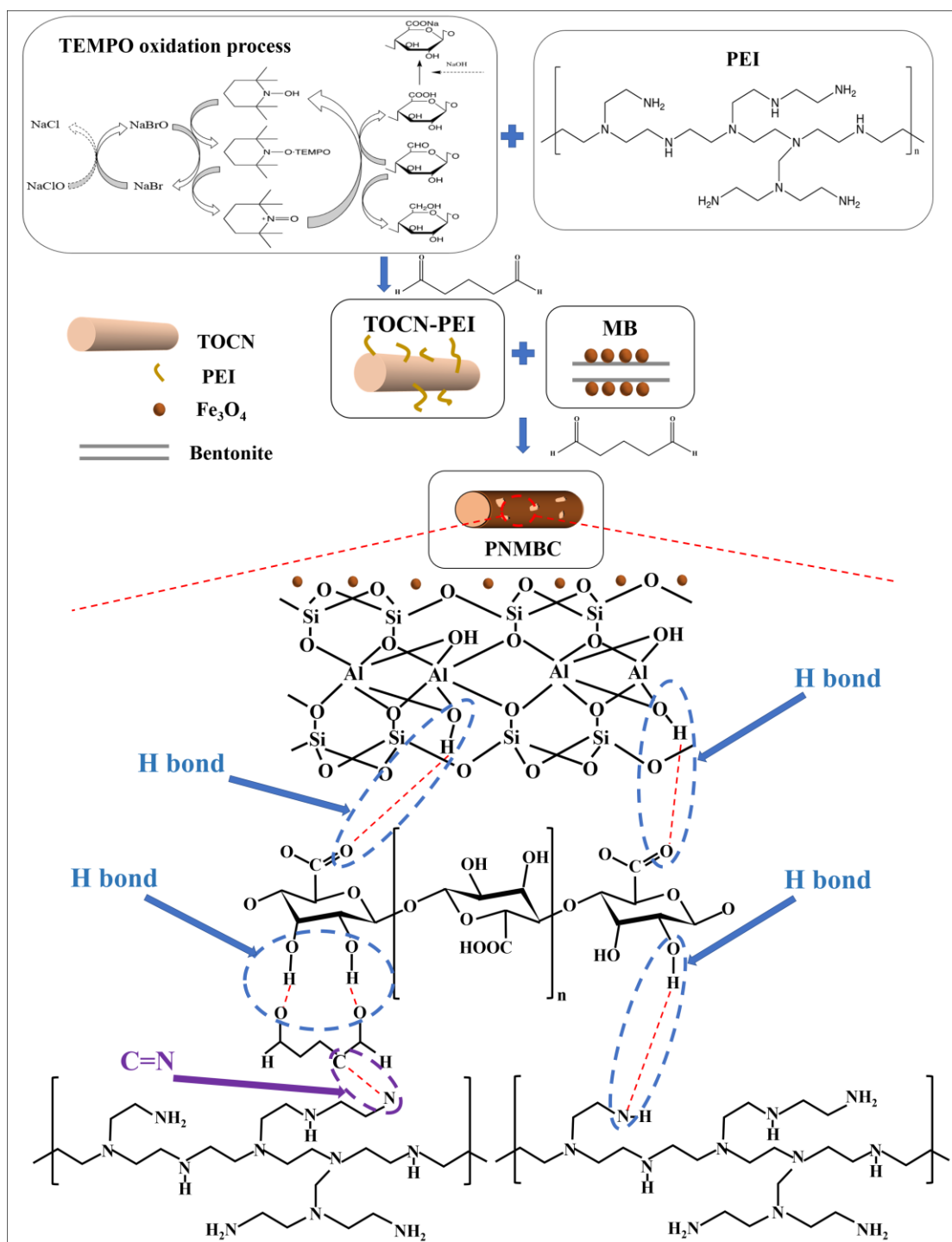


Figure 1. Schematic diagram of synthetic PNMBC biosorbent.

2.6. Characterization

The composites were analyzed using Fourier transform infrared spectroscopy (FT-IR, Tensor 27, Bruker, Ettlingen, Germany), X-ray diffraction (XRD, Bruker D8, Ettlingen, Germany), and thermogravimetric analysis (TGA, TGA 5500, New Castle, PA, USA). The surface morphology of each material was analyzed using scanning electron microscopy

(SEM, JSM-7800F, JEOL Ltd. Beijing, China). The surface area and void characterization of the biosorbent was characterized by Brunauer–Emmett–Teller analysis (McASAP2460).

2.7. Batch Adsorption Test

The adsorption performance of the composites on Cu(II) was evaluated by the static adsorption method. A certain amount of anhydrous copper sulfate was dissolved in ultrapure water, and samples of different concentrations were obtained using the gradient dilution method. The pH was adjusted with aqueous NaOH (1 M) and HCl (1 M) solutions. PNMBC (0.01 g) was added to the prepared Cu(II) solution and shaken at 180 rpm for 60 min at a constant temperature of 25 °C. Finally, the supernatant was collected through a 0.45- μ m filter membrane, and the concentration of Cu(II) was determined by atomic absorption spectrometry (AAS, WFX-120, Shanghai Reunion Scientific Instrument Co., Ltd. Shanghai, China). The adsorption capacity and removal efficiency of Cu(II) were calculated with the following equations [30]:

$$q_t = (C_0 - C_e) \times \frac{V}{m} \quad (1)$$

$$\varepsilon = \left(1 - \frac{C_e}{C_0}\right) \times 100 \quad (2)$$

where C_0 and C_e (mg/L) are the initial and equilibrium concentrations, respectively, V (L) is the volume of the solution, m (g) is the weight of the adsorbent, and ε is removal efficiency.

The adsorption kinetics of PNMBC were identified by determining their q_t values with increasing adsorption time at the fixed C_0 (100 mg/L) and solution pH 5.0, with mass ratios of 1:1 and 1:2, and pH 4.0 with a mass ratio of 2:1 of the prepared solutions at 25 °C, and fitting them to three kinetic models:

$$\text{(pseudo-first-order)} \quad \ln(q_e - q_t) = \ln q_e - k_1 t \quad (3)$$

$$\text{(pseudo-first-order)} \quad \frac{t}{q_t} = \frac{1}{k_2 q_e^2} + \frac{t}{q_e} \quad (4)$$

where q_e (mg/g) and q_t (mg/g) are the Cu(II) adsorption capacities at equilibrium and time t (min), k_1 (min^{-1}) and k_2 ($\text{g}/(\text{mg} \cdot \text{min})$) are the rate constants [31].

The q_e values of PNMBC (25 °C) were also determined by varying C_0 and temperature at the fixed solution pH, and were then fitted to two isotherm models [11,32]:

$$\text{(Langmuir model)} \quad \frac{C_e}{q_e} = \frac{1}{q_m} + \frac{1}{K_L q_m C_e} \quad (5)$$

$$\text{(Freundlich model)} \quad \ln q_e = \frac{\ln C_e}{n} + \ln K_F \quad (6)$$

where C_e is the Cu(II) concentration of the solution at the equilibrium state, q_m (mg/g) and q_e (mg/g) are the maximum and equilibrium adsorption capacities, respectively, K_L is the Langmuir constant, K_F is the Freundlich constant, and n is the heterogeneity factor.

The standard Gibbs free energy ΔG (kJ/mol), enthalpy ΔH (kJ/mol), and entropy ΔS (J/mol·K) changes of adsorption were obtained from thermodynamic relationship calculations [33,34]. In this paper, the effect of temperature (15 °C, 25 °C, and 35 °C) on the adsorption of Cu(II) onto PNMBC was investigated.

$$k_D = \frac{q_e}{c_e} \quad (7)$$

$$\ln k_D = \frac{\Delta S}{R} - \frac{\Delta H}{RT} \quad (8)$$

$$\Delta G = \Delta H - T\Delta S \quad (9)$$

where k_D (L/Kg) is the adsorption partition coefficient, R is the gas constant (8.314 J/mol·K), T (K) is the Kelvin temperature, and ΔH and ΔS values are the slope and intercept of the straight line in the graph of the $\ln k_D - T^{-1}$ relationship, respectively.

3. Results and Discussion

3.1. Characterization of PNMBC

3.1.1. FT-IR Analysis

The FT-IR spectra of the modified nanocellulose and the biosorbent PNMBC are shown in Figure 2. The absorption peak of TOCN-PEI at 1660 cm^{-1} is due to the stretching vibration of the C=N group formed during the cross-linking of the hydroxyl group of nanocellulose with the amine group of PEI, indicating the successful cross-linking of PEI with TOCN [25]. The characteristic peaks in the range of $1050\text{--}1100\text{ cm}^{-1}$ (C–O–C vibration), 1160 cm^{-1} (C–O–C stretching of β -glycosidic linkage), 1310 cm^{-1} (–COOH vibration), 1433 cm^{-1} (–CH₂ bending vibrations or –COO– symmetric stretching vibrations of the carboxyl group in the form of salt), 1630 cm^{-1} (asymmetric COO[–] stretching vibrations of carboxyl group, $V_{\text{asym}}(\text{COO}^-)$), 2886 cm^{-1} (–CH aliphatic stretching vibrations), and 3336 cm^{-1} (–OH stretching vibrations) are the cellulose absorption peaks [35]. For magnetic bentonite, the dominant band of $\alpha\text{-Fe}_2\text{O}_3$ appears around 472 and 570 cm^{-1} , and the peaks at 1637 cm^{-1} and 3382 cm^{-1} refer to the Al–OH and Si–OH stretching vibrations and montmorillonite outer layer –OH stretching vibration, respectively [36].

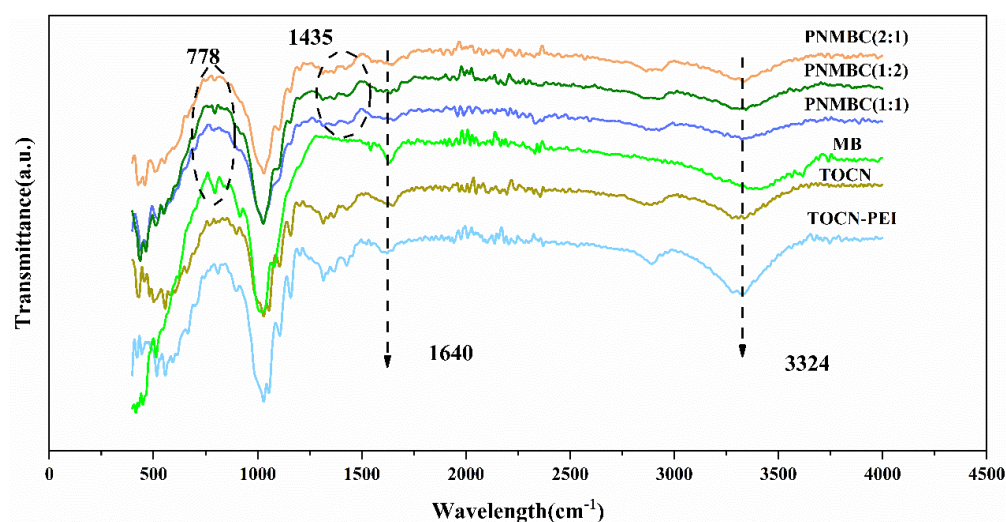


Figure 2. FT-IR spectra of the modified nanocellulose and PNMBC biosorbent: 2:1, 1:2, and 1:1 refer to the different mass ratios of PEI-modified TEMPO cellulose nanoparticles (TOCN-PEI) and magnetic bentonite (MB).

Compared to TOCN-PEI and magnetic bentonite, wide peaks at 3324 cm^{-1} are observed for the three prepared composites, indicating the corresponding O–H peaks of the biosorbents and the formation of hydrogen bonds. The intensity of the C=O stretching peak at 1640 cm^{-1} of the three adsorbents was reduced compared to that for TOCN-PEI, indicating the interaction between the C=O group and the clay [37]. Since the Al(III) cation at the center of the bentonite octahedral layer exhibits Lewis acid properties, the acidic site can interact with the –NH₂ group of PEI [38,39], resulting in a slightly weaker absorption peak of –NH₂ at 1435 cm^{-1} of the composites than the TOCN-PEI fraction, thus indicating that the amino groups in the bentonite and TOCN-PEI interact through the hydrogen bond, and the successful cross-linking of the magnetic bentonite with TOCN-PEI [40]. In addition, the typical N–H bond stretching and bending bands at 3400 cm^{-1} and 1435 cm^{-1} overlap with the Si–O band [41], and the absorption peaks between 553 cm^{-1} and 613 cm^{-1} were ascribed to the stretching vibration of Fe–O in Fe₃O₄ [42,43]. It was found that the magnetic bentonite was successfully introduced into the structure of TOCN-PEI.

3.1.2. XRD Analysis

The XRD analysis results for PNMBC are shown in Figure 3. The 2θ peaks at 19.72° and 21.96° are characteristic of the bentonite crystalline phase. The peaks at 30.3° , 35.6° , 43.4° , 57.3° , and 62.9° correspond to (220), (311), (400), (511), and (440) of Fe_3O_4 [44]. This indicates that the magnetic bentonite was successfully prepared. The 2θ peaks at 14.13° , 22.6° , and 34.32° are the characteristic peaks of cellulose I_β crystal planes 101, 200, and 040, respectively [45]. In contrast to the crystalline peaks of TOCN-PEI, two distinctive peaks appear for the composite PNMBC at 19.8° and 21.9° , which indicate that part of the cellulose type I was transformed into cellulose type II during the preparation of the composite [46,47]. In conclusion, the TOCN-PEI/magnetic bentonite composite was successfully synthesized.

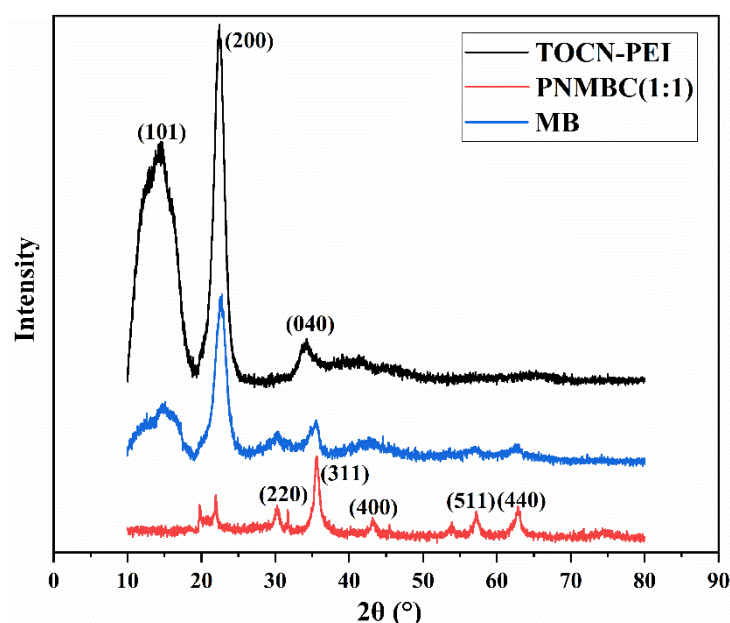


Figure 3. XRD results of the PEI-modified nanocellulose and prepared composites.

3.1.3. SEM Analysis

The morphologies of the composites before and after adsorption of Cu(II) are shown in Figure 4. The experiment results show that the white cellulose becomes dark brown, which can confirm the penetration of bentonite particles into the cellulose fiber (the zoomed out figure in Figure 4a). The modified nanocellulose has a rod-like structure with a maximum diameter of $40\ \mu\text{m}$ (Figure 4a). The magnified composite image has a rough and dry surface morphology with obvious voids and pores regarding the morphology of the nanocellulose. In contrast, the particles on the rod-like cellulose surface are seen to be agglomerated as a whole, and the unevenly sized stomata structure was observed on the surface of the PNMBC, which is consistent with the result obtained by Xing et al. [48]. During the experiment, PNMBC was able to disperse more uniformly in water, which could enhance the contact opportunities with Cu(II) and improve the adsorption efficiency. These pores of different shapes and sizes were able to easily encapsulate Cu(II) . Meanwhile, the presence of abundant chemical functional groups with strong adsorption activities on the material surface also promoted the adsorption performance [28,39]. It was observed that the aggregate structure on the surface of the adsorbent becomes larger after adsorption. In addition, a rough surface was observed on the composite adsorbent after the adsorption of Cu(II) , which was rougher compared to the original PNMBC, indicating that Cu(II) was deposited on the surface of the adsorbent after adsorption.

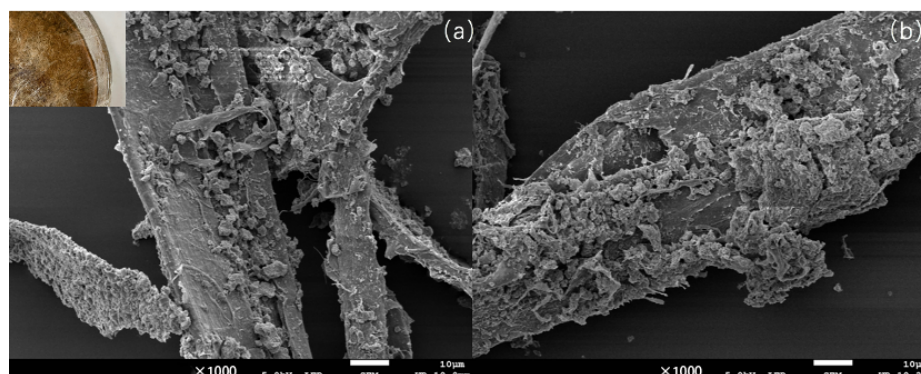


Figure 4. SEM images of PNMBC before (a) and after (b) adsorption of Cu(II).

3.1.4. TG Analysis

The results of TGA and DTG analysis of the prepared biosorbent, ranging from 50 to 750 °C, are shown in Figure 5. The first weight loss phase occurred between 30–100 °C with a weight loss of 5.133%, which was due to the loss of adsorbed water of the composite. The second weight loss phase was between 60–350 °C, which was probably due to the combustion loss of organic matter, with a weight loss of 37.887%. When the temperature rose to 750 °C, the weight loss of PNMBC (1:1) was 15.238%, which was mainly due to the mass loss caused by the decomposition of the components C, H, and N of the PNMBC, indicating the successful grafting of PEI onto the TOCN particle [19]. The residual mass fraction of the PNMBC was about 40%. The prepared biosorbent exhibited a high thermal stability, indicating a good performance in practical application.

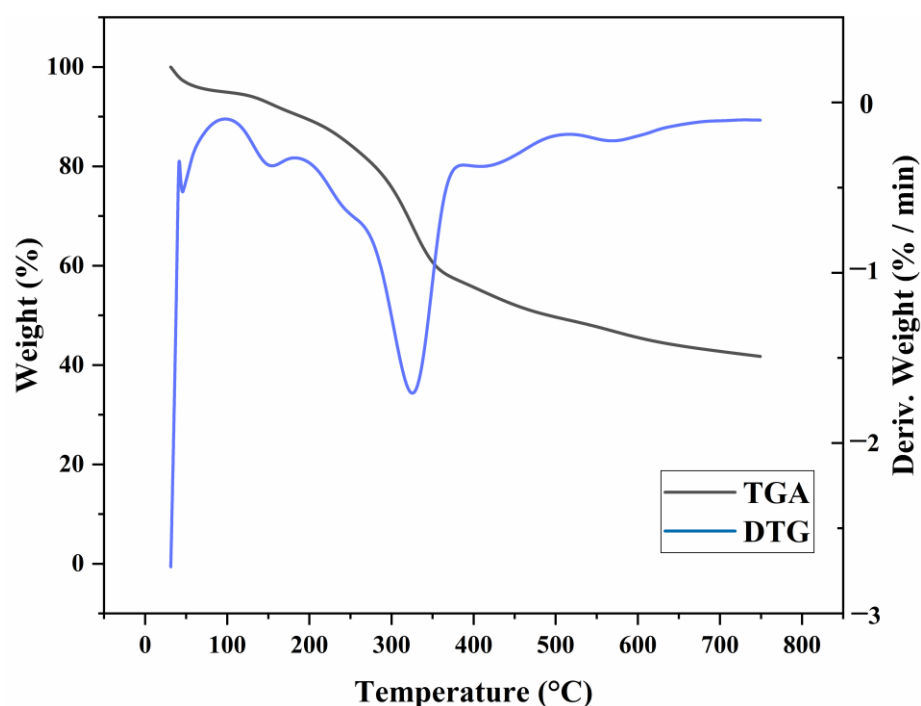


Figure 5. Thermal stability of the PNMBC biosorbent (TOCN–PEI:MB = 1:1).

3.1.5. BET Analysis

The N₂ adsorption–desorption curves of the PNMBC biosorbent are shown in Figure 6. According to the IUPAC classification rule, the isotherm is type IV, and the adsorption–desorption loop is a typical H₃-type hysteresis [37,49], indicating the possible existence of crack-like pores, i.e., three-dimensional interconnected pores, indicating the cross-link of the organic–inorganic polymer. When the relative pressure P/P₀ was in the low pressure

region of 0~0.8, the adsorption of N_2 increased slowly. In contrast, when the relative pressure P/P_0 was in the high pressure region of 0.8~1.0, the adsorption of N_2 increased sharply, indicating that a small amount of microporosity was formed in the composite due to the presence of linear PEI, which is consistent with the SEM result. The specific surface area of the sample was relatively low, at $14.246 \text{ m}^2/\text{g}$, which was due to the deposition of Fe_3O_4 into the mesopores of the bentonite particle, blocking the exposed surface. In Figure 6b, it can be seen that the highest pore diameter was around 7 nm, indicating the presence of the mesoporous structure of the PNMBC biosorbent.

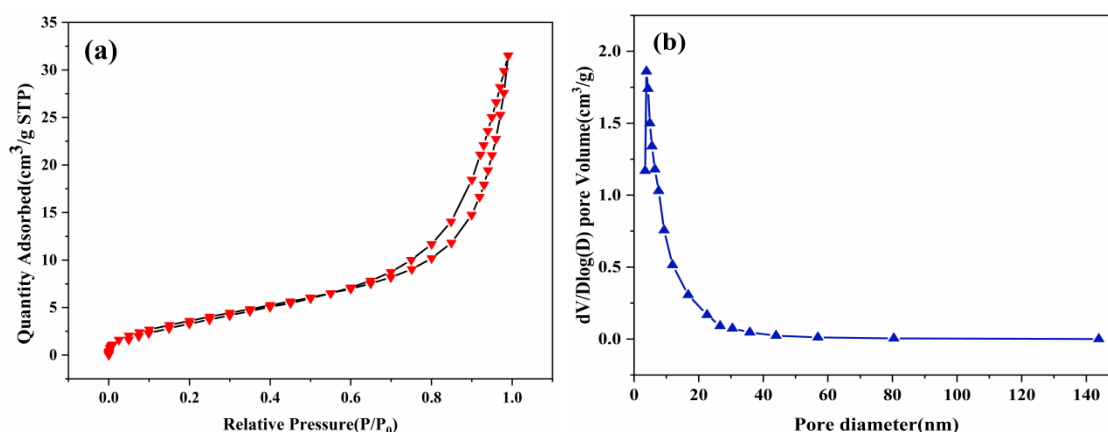


Figure 6. BET analysis of PNMBC (TOCN-PEI:MB = 1:1): (a) N_2 adsorption–desorption curves and (b) pore size distribution.

3.1.6. Zeta Potential

The pH can significantly change the surface function of the adsorbent, which affects the protonation of organic functional groups in the composite and the migration of metal ions in water. When the pH ranged from 2 to 5, the Cu(II) ion existed in the form of $Cu(II)$ and $Cu(OH)^+$. When the pH was >5 , the precipitation of $Cu(OH)_2$ occurred in the solution. Thus, the adsorption experiment was carried out with pH ranging from 2 to 5. As shown in Figure 7a, the zeta potentials of the composites were all positively charged when the pH was below 4.2, and the electronegativity increased with the increase in pH. Figure 7b demonstrates the adsorption effect of the biosorbent on Cu(II) at different pH. It was found that the adsorption efficiency of composites 1:1 and 1:2 gradually increased with increasing pH, reaching maximum adsorption efficiency at pH 5.0. The adsorption efficiency reached the highest levels at pH 4 with the biosorbent (TOCN-PEI:MB = 2:1). Comparing the zeta potential in Figure 7a, it can be seen that at $pH < 4.2$, the presence of PEI led to a large amount of positively charged amino groups in the composites, and the protonation of amino groups $-NH_2^+$ and $-NH_3^+$ occurred at low pH [50]; once protonated, these groups compete with the cationic copper ions [51], resulting in relatively low adsorption efficiencies. Therefore, at pH 2~4, the surface was positively charged due to the deprotonation of surface amino groups, and there were fewer negatively charged adsorption sites on the surface of the composite; electrostatic repulsion also prevented Cu(II) adsorption. In comparison, at $pH > 4.2$, the surface of biosorbents (1:1 and 1:2) were negatively charged, and the adsorption of Cu(II) increased via electrostatic interaction. However, the adsorption efficiency of composite 2:1 decreased, which was probably due to the increased positive charge of the composite contributed by a large proportion of TOCN-PEI [52]. Therefore, composite 2:1 reached a higher adsorption efficiency at pH 4.0, indicating that electrostatic force is not the only force affecting the adsorption of Cu(II). Therefore, in order to achieve a high adsorption efficiency in the actual treatment of water containing Cu(II), pH 5.0 was chosen for composites 1:1 and 1:2, and pH 4.0 was set for composite 2:1, as the optimal pH of the solution for the subsequent adsorption study.

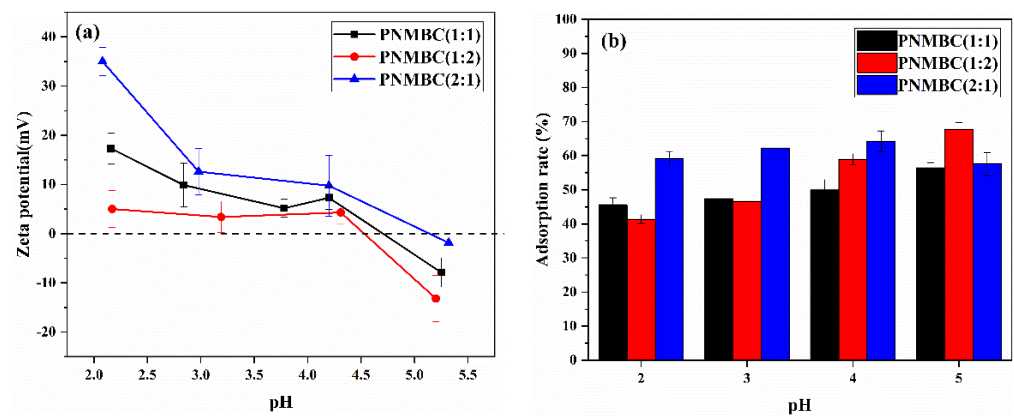


Figure 7. (a) Zeta potential of PNMBC biosorbent and (b) the adsorption efficiencies at different pH levels.

3.2. Effect of Batch Adsorption Performance

3.2.1. Effect of Biosorbent Dosage

The adsorption capacities with different dosages of 0.01 g, 0.02 g, 0.05 g, 0.08 g, and 0.1 g of PNMBC composite were investigated using a Cu(II) concentration of 100 mg/L. As can be seen in Figure 8, with the increase in adsorbent dosage, the adsorption capacities decrease. This phenomenon may be due to the increased adsorption site of the biosorbent [53,54]. The maximum adsorption capacity of Cu(II) was achieved for three different ratios of PNMBC composites at a dosage of 0.01 g, reaching 281.3 mg/g (1:1), 246.76 mg/g (1:2), and 234.12 mg/g (2:1), respectively. Therefore, the adsorbent dosage of 0.01 g for all of the three composites was considered to be the optimal mass in the subsequent experiment.

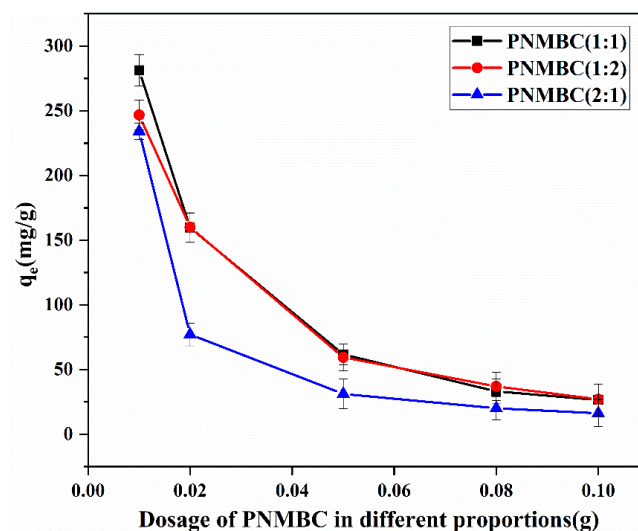


Figure 8. Effect of PNMBC biosorbent dosage on the adsorption of Cu(II).

3.2.2. Effect of Initial Concentration of Cu(II)

The effect of initial concentration of Cu(II) (50 mg/L, 100 mg/L, 150 mg/L, 200 mg/L, 300 mg/L, 400 mg/L, and 500 mg/L) with the conditions of adsorbent dosage 0.01 g, pH 5 (1:1 and 1:2) and 4 (2:1), and an adsorption time of 2 h is shown in Figure 9. The results show that the highest adsorption capacities of PNMBC for Cu(II) were 491.2 mg/g (1:1), 490.65 mg/g (1:2), and 446.5 mg/g (2:1) at 35 °C. The highest adsorption capacities of PNMBC for Cu(II) were 594.1 mg/g (1:1), 510.2 mg/g (1:2), and 490.75 mg/g (2:1) at 25 °C. The highest adsorption capacities of PNMBC for Cu(II) were 757.45 mg/g (1:1), 692.85 mg/g (1:2), and 563.3 mg/g (2:1) at 15 °C. The adsorption capacity was higher than that of the other modified cellulose-based adsorbents (Table 1). It was found that the

adsorption capacity increased as the Cu(II) concentration increased. However, with the increase in concentration, the adsorption capacity gradually reached saturation, probably due to the gradual substitution of adsorption sites on the biosorbent. In addition, the increase in the heavy metal concentration gradient could have inhibited the driving force of the heavy metal mass transfer in the liquid and solid phases, resulting in an increase in isothermal adsorption until the biosorbent reaches saturation [55].

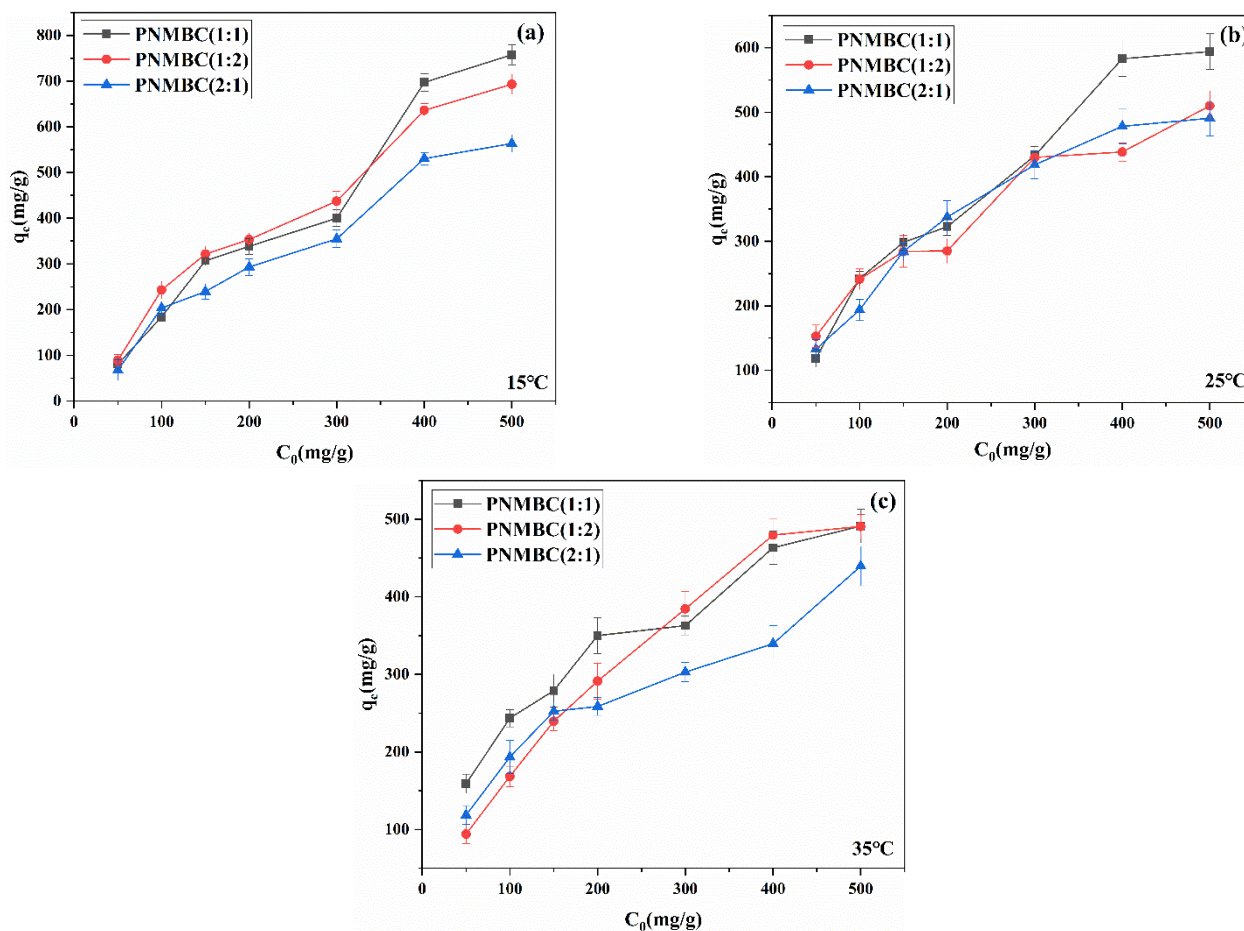


Figure 9. Effect of different initial concentrations of Cu(II) adsorption at (a) 15 °C, (b) 25 °C, and (c) 35 °C.

Table 1. The Cu(II) adsorption capacity of nanocellulose-modified and bentonite-based adsorbents obtained from the literature.

Adsorbent	Pollutant	Maximum Adsorption Capacity (mg/g)	Reference
CMCNFs	Cu(II)	115.3	[22]
PEI-BC	Cu(II)	148	[23]
TOCN-PEI	Cu(II)	52.32	[28]
BC/GO	Cu(II)	65	[30]
cellu/cys-bent	Cu(II)	32.36	[39]
MKC	Cu(II)	16.5	[41]
Fe ₃ O ₄ /ATP@(BCNs/CS)	Cu(II)	70.5	[44]
TCP	Cu(II)	109.89	[48]
PNMBC	Cu(II)	757.45	This work

The adsorption isotherms of the Freundlich model and Langmuir model are shown in Figure 10, and the fitted parameters are shown in Table 2. The results show that the R^2 of the Freundlich model was higher compared to the Langmuir model, indicating that the adsorption equilibrium data were well-fitted with the Freundlich model and the adsorption process was multilayered and non-uniform.

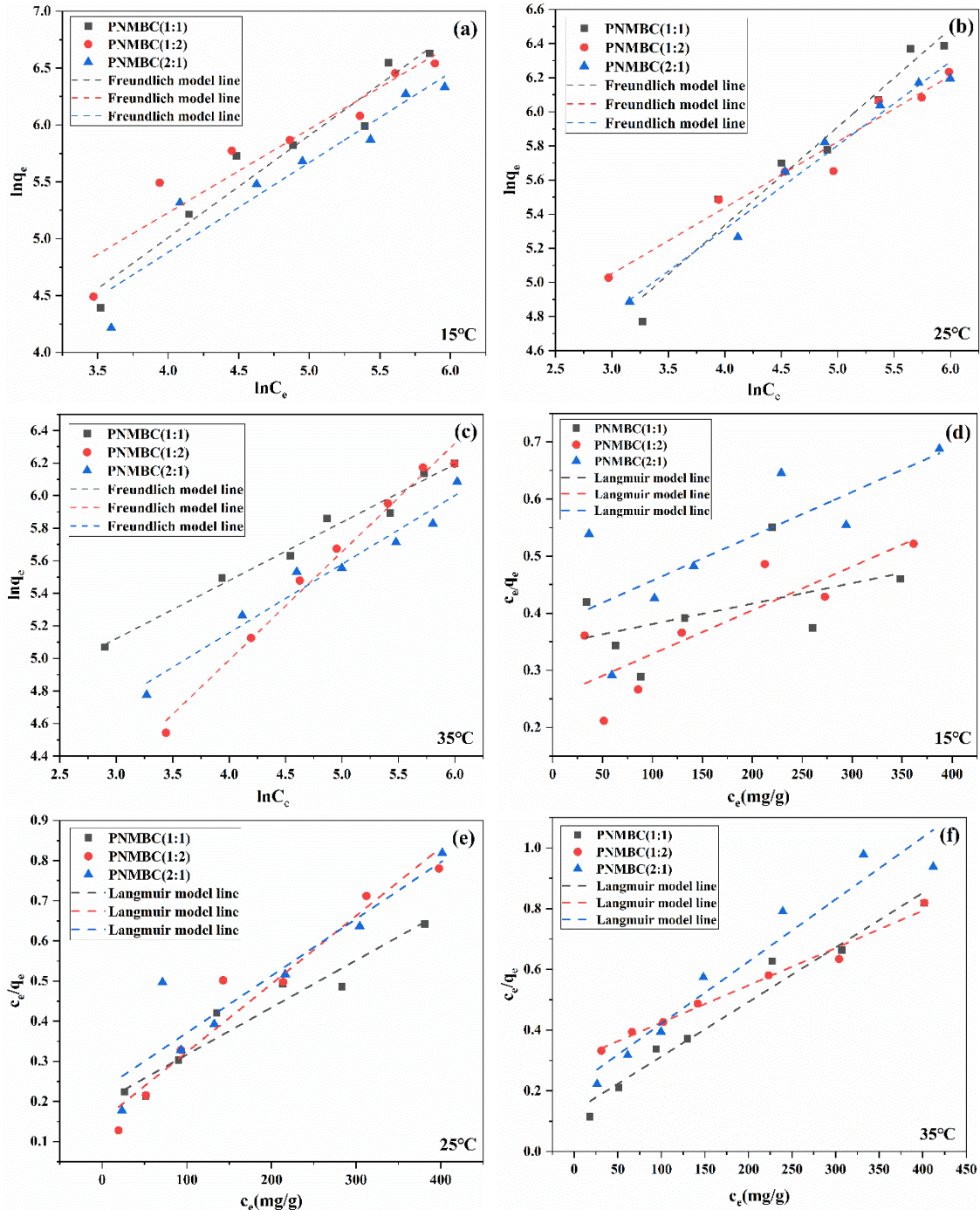


Figure 10. Isotherm fitted curves of PNMBBC composites (TOCN–PEI:MB = 1:1, 1:2, and 2:1 for Cu(II)) adsorption: (a–c) Freundlich fits and (d–f) Langmuir fits.

Table 2. Adsorption isotherm constants for Cu(II) adsorption by PNMBC at different temperatures.

Composite	Temperature (°C)	Langmuir Models			Freundlich Models		
		Q_{max} (mg/g)	K_L (L/mg)	R^2	n	K_F (mg/g)(L/mg) ^{-1/n}	R^2
1:1	15	2790.02	0.00104	0.09003	1.20	5.84	0.90881
	25	847.45	0.00593	0.91955	1.96	29.31	0.93284
	35	555.55	0.0135	0.96048	2.79	57.35	0.96510
1:2	15	1306.5	0.00304	0.64308	1.56	16.14	0.93969
	25	588.23	0.0110	0.93572	2.51	46.37	0.95370
	35	813.01	0.00400	0.98150	1.69	15.25	0.98320
2:1	15	1288.95	0.00204	0.47880	1.45	9.72	0.94024
	25	704.22	0.00600	0.82663	2.31	38.94	0.94024
	35	487.80	0.00900	0.92437	2.41	33.39	0.93280

3.2.3. Effect of Adsorption Time

The results show that the adsorption capacity of Cu(II) reached saturation in 5 min for the three PNMBC biosorbents at 25 °C (Figure 11b), indicating rapid adsorption of Cu(II). The adsorption reached equilibrium in 10 min at 15 °C and 35 °C for the three PNMBC biosorbents (Figure 11a,c). It was found that the PNMBC biosorbent of 2:1 has a lower adsorption capacity compared with the other two PNMBC biosorbents, and the biosorbent with 1:1 (TOCN–PEI:MB) had the optimum ratio regarding the preparation of the composite. However, the results show that the biosorbent with 1:2 was the most suitable composite in the adsorption of Cu(II) at high temperature (35 °C).

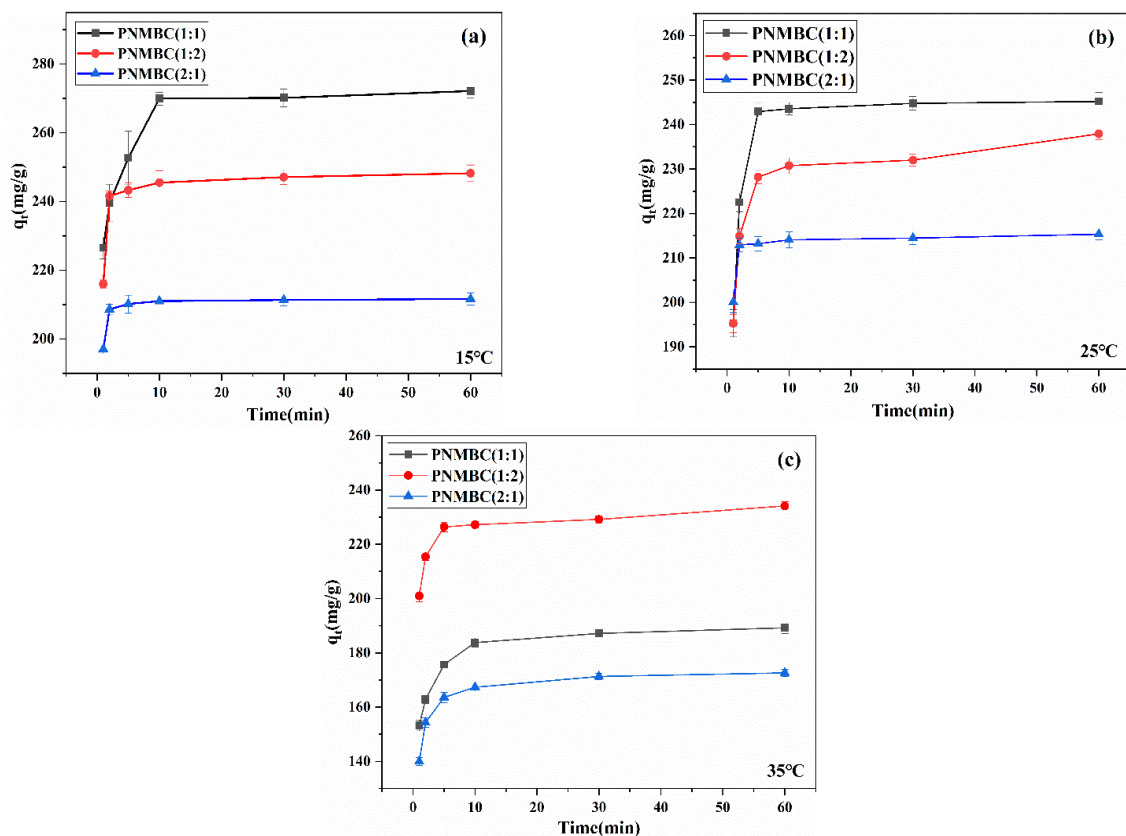


Figure 11. Effect of different ratios of PNMBC (1:1, 1:2, and 2:1) on the adsorption of Cu(II) at different contact times: (a) 15 °C, (b) 25 °C, and (c) 35 °C.

Figure 12 shows the data of the pseudo-first-order kinetic model and the pseudo-second-order kinetic model, and the data fitting parameters are shown in Table 3. The correlation coefficients, R^2 , of the pseudo-second-order kinetic model for the three different ratios of biosorbents were much higher than that of the pseudo-first-order kinetic model. Meanwhile, the q_e calculated by the secondary kinetic model was similar to the actual value, indicating that the adsorption process follows the pseudo-second-order kinetic model. Therefore, it can be concluded that the adsorption process of Cu(II) by PNMBC is mainly controlled by chemical adsorption [50].

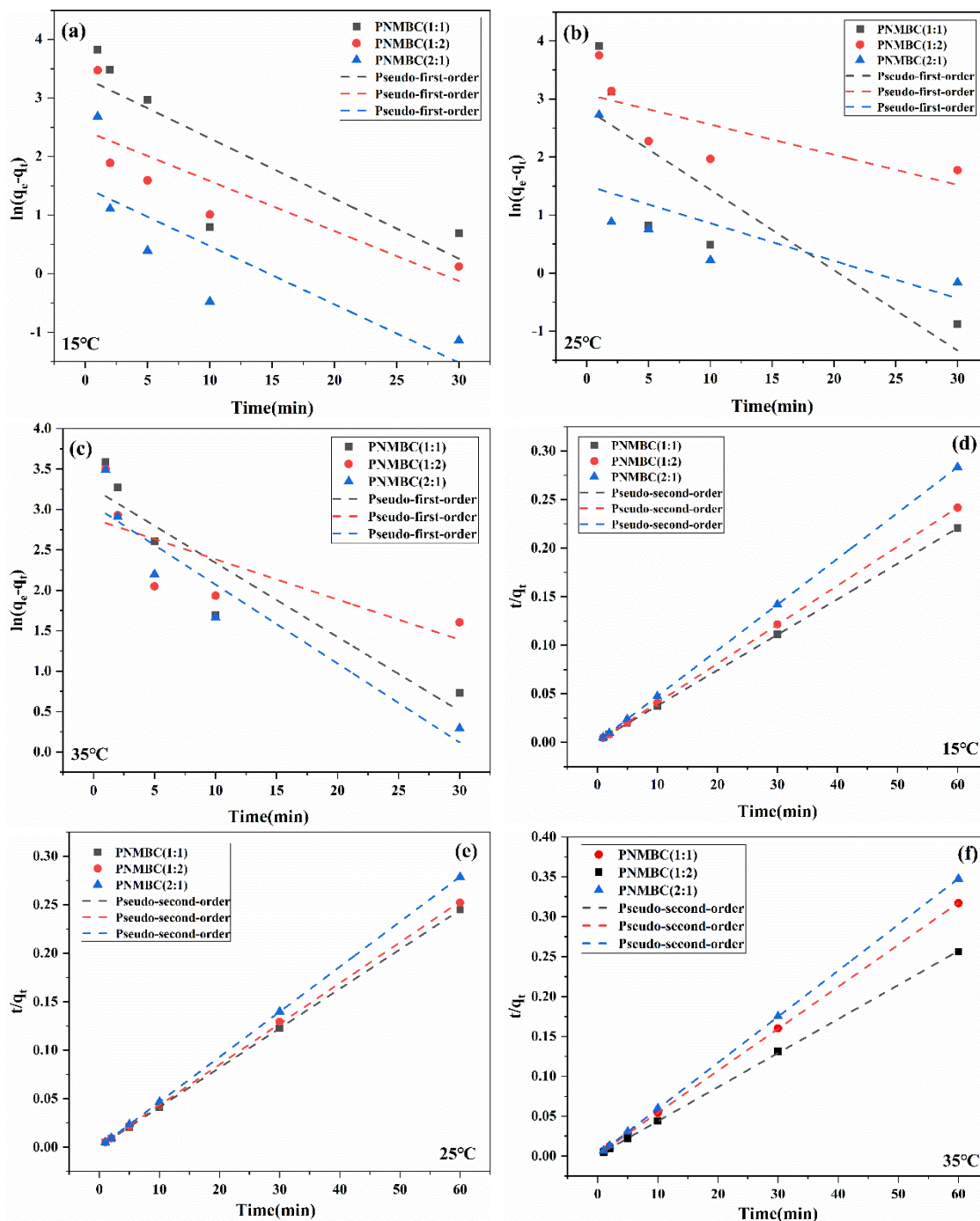


Figure 12. Kinetic fitted curves for Cu(II) adsorption by TOCN-PEI:MB (1:1, 1:2, and 2:1): (a–c) pseudo-first-order and (d–f) pseudo-second-order.

Table 3. Kinetic fitting parameters of PNMBC for Cu(II) adsorption.

Composite	Temperature (°C)	Pseudo-First-Order Adsorption Kinetics			Pseudo-Second-Order Adsorption Kinetics		
		K ₁ (min ⁻¹)	Q _e (mg/g)	R ²	K ₂ (g/(mg·min))	Q _e (mg/g)	R ²
1:1	15	0.102	28.20	0.55969	0.013	273.22	0.99998
	25	0.14	16.82	0.60238	0.026	245.70	0.99999
	35	0.091	25.95	0.82591	0.015	190.11	0.99998
1:2	15	0.085	11.44	0.57244	0.033	248.76	1
	25	0.052	21.76	0.39796	0.014	238.09	0.99985
	35	0.049	17.84	0.42768	0.016	234.19	0.99989
2:1	15	0.099	4.34	0.52444	0.098	211.86	1
	25	0.065	4.51	0.31011	0.073	215.52	1
	35	0.098	21.06	0.86403	0.019	173.31	0.99999

3.2.4. Effect of Temperature

The results show that the adsorption capacity decreases with the increase in temperature, and that adsorption is an exothermic process. The data in Table 4 indicate that the adsorption of Cu(II) by the composite was a spontaneous process, and the increase in temperature could enhance the degree of spontaneity [56]. The absolute value of ΔG decreased with increasing temperature, indicating that the adsorption process of Cu(II) was spontaneous, and high temperature was not conducive to adsorption [57]. The value $\Delta S < 0$ indicates that the adsorption was an entropy-decreasing process, i.e., it increased the randomness of Cu(II) at the solid–liquid interface. The value $\Delta H < 0$ indicates that the biosorbent adsorption was an exothermic process, and the increase in temperature led to an increase in ion mobility, while the diffusion of adsorbed ions to the outer boundary layer increased the ionic entropy, thus increasing the resistance of Cu(II) adsorption. Therefore, decreasing the temperature favored the adsorption efficiency of Cu(II).

Table 4. Thermal parameters for the adsorption of Cu(II).

Composite	ΔG (KJ/mol)			ΔH (KJ/mol)	ΔS (J/mol·K)
	15 °C	25 °C	35 °C		
1:1	−4.335	−3.625	−2.916	−24.774	−70.97
1:2	−3.777	−3.762	−3.748	−4.195	−1.451
2:1	−3.268	−2.964	−2.660	−12.022	−30.399

3.3. Adsorption Mechanism

It was found that the adsorption of Cu(II) was effective for PNMBC 1:1 and 1:2 composites at pH 4, and the electrostatic attraction between the proton–amine group of PNMBC and Cu(II) played a leading role in the adsorption of Cu(II). In contrast, the adsorption of Cu(II) for PNMBC 2:1 was relatively low, which is because the increase in TOCN–PEI led to an increase in positively charged amino groups. In addition, the increase in linear PEI molecules grafted onto the nanocellulose fiber decreased the number of surface micropores of the PNMBC. Finally, the adsorption kinetics and thermodynamic data indicate that the adsorption of Cu(II) was a chemical process, i.e., Cu(II) was chelated with the functional groups on the surface of PNMBC and formed a non-uniform multimolecular layer. This is consistent with other studies, such as the large adsorption capacities of metal–organic frameworks (MOFs) on nanofiber materials are mainly owing to the interaction between the target ions with the functional binding groups on the composite [58]. Additionally, heavy metal ions were rapidly adsorbed onto the material surface through the chemical process

with various functional groups (e.g., $-\text{NH}_2$, $-\text{OH}$, $-\text{CO}_2\text{H}$, $-\text{SO}_3\text{H}$) [59,60]. Meanwhile, it can be seen from Figure 13 that the biosorbent composite with the addition of magnetic bentonite not only exhibited an efficient adsorption performance for Cu(II), but also that the blue Cu(II) solution had clarified after 60 min and showed a strong effect on the efficiency of magnetic separation of PNMBC biosorbent. Overall, the PNMBC adsorption process consists of three main stages: (1) the membrane diffusion phase of mass transfer, where the metal ions reach to the surface of PNMBC through the aqueous membrane, (2) the diffusion of metal ions in the PNMBC pores, and (3) the occurrence of electrostatic attraction and chemisorption to occupy the adsorbent surface position [61].

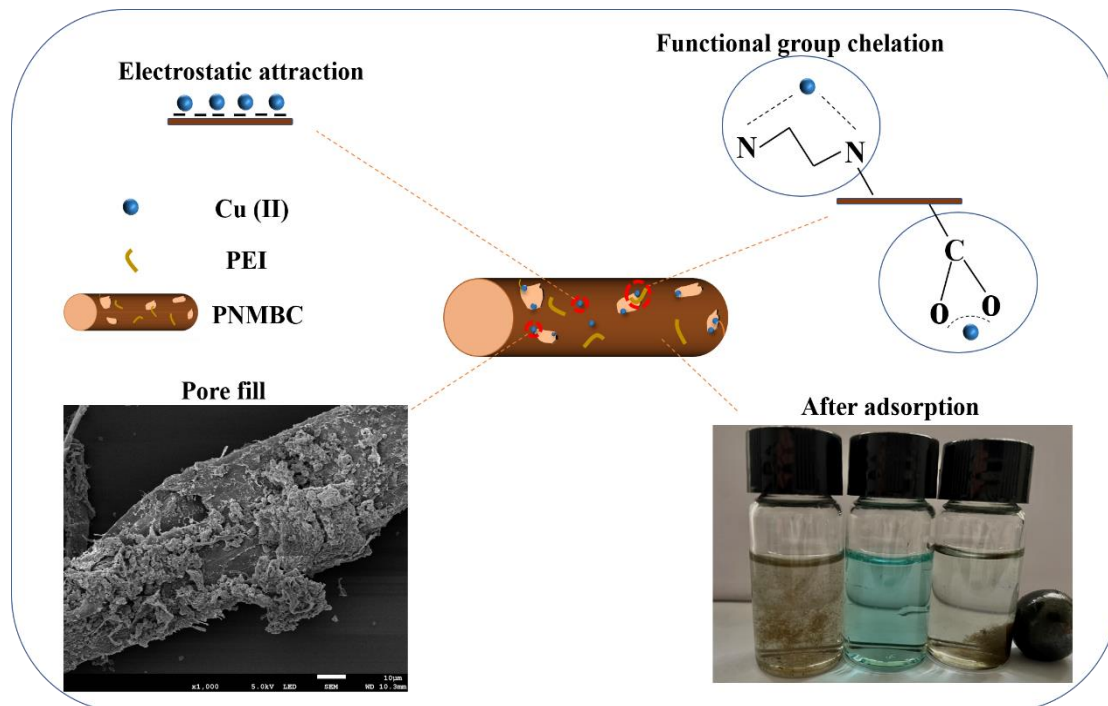


Figure 13. Mechanism of Cu(II) adsorption by the PNMBC biosorbent.

3.4. Reusability of PNMBC

In practical use, the adsorbent should not only have a high adsorption capacity, it should also have high reusability. In this paper, three repeated cycles of adsorption–desorption experiments were conducted to monitor the adsorption performance of PNBBC for Cu(II). After each experiment, PNMBC was separately washed by 1 mol/L NaOH for recycling. The results are shown in Figure 14, the adsorption amount of Cu(II) on PNBBC decreased with the increase in adsorption–desorption times. After four cycles at 15 °C, the adsorption capacities of PNMBC (1:1, 1:2, 2:1) for Cu(II) reached 81.26 mg/L, 70.7 mg/L, and 75.85 mg/L, respectively. The adsorption capacity after four cycles was still stronger than that of most adsorbents (Table 1). The decrease in the adsorption capacity of the second cycle may be due to the irreversible binding of some active sites of PNBBC to Cu(II), thereby reducing the binding site density of Cu(II) [19]. Our reusability studies show that PNMBC has the potential to be used for Cu(II) processing.

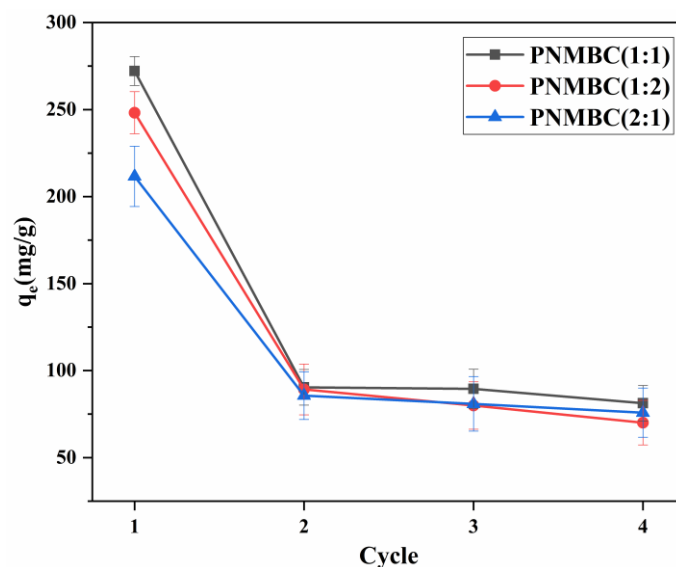


Figure 14. Adsorption–desorption cycles for Cu(II) removal by PNMBC.

4. Conclusions

The optimal ratio of the biosorbent for Cu(II) adsorption was determined by changing the ratio of TOCN–PEI to magnetic bentonite. The optimum conditions for the adsorption of Cu(II) were as follows: a 1:1 ratio of TOCN–PEI to MB, pH 5, and a reaction time of 10 min at 15 °C. Our results show that the adsorption was well-fitted with the Freundlich model, and that the adsorption was a multilayer non-uniform chemical process. The maximum adsorption capacity of Cu(II) reached 757.45 mg/g. In addition, the biosorbent exhibited a good magnetic separation performance for continuous application. This study provides a fabrication method for the preparation of modified nanocellulose biosorbent, which exhibited a high removal efficiency for Cu(II) from water.

Author Contributions: X.S.: Methodology, Writing-original draft and editing, Funding acquisition. X.L.: Software, Resources, Writing-original draft. C.H.: Formal analysis, Data curation. L.B.: Conceptualization, Editing. T.W.: Formal analysis, Visualization. Y.S.: Conceptualization, Methodology, Supervision, Editing. All authors have read and agreed to the published version of the manuscript.

Funding: This research work was financially supported by the Shaanxi Natural Science Fund (2021SF-503) and the National Key Research and Development Program of China (2020YFC1808304, 2020YFC1808300).

Institutional Review Board Statement: Not applicable.

Informed Consent Statement: Not applicable.

Data Availability Statement: Not applicable.

Conflicts of Interest: The authors declare they have no conflict of interest.

References

- Wong, S.M.; Zulkifli, M.Z.A.; Nordin, D.; Teow, Y.H. Synthesis of cellulose/nano-hydroxyapatite composite hydrogel absorbent for removal of heavy metal ions from palm oil mill effluents. *J. Polym. Environ.* **2021**, *29*, 4106–4119. [[CrossRef](#)]
- Kameda, T.; Suzuki, Y.; Yoshioka, T. Removal of arsenic from an aqueous solution by coprecipitation with manganese oxide. *J. Environ. Chem. Eng.* **2014**, *2*, 2045–2049. [[CrossRef](#)]
- Radchenko, V.; Engle, J.W.; Wilson, J.J.; Maassen, J.R.; Nortier, F.M.; Taylor, W.A.; Birnbaum, E.R.; Hudston, L.A.; John, K.D.; Fassbender, M.E. Application of ion exchange and extraction chromatography to the separation of actinium from proton-irradiated thorium metal for analytical purposes. *J. Chromatogr. A* **2015**, *1380*, 55–63. [[CrossRef](#)] [[PubMed](#)]
- Sunil, K.; Karunakaran, G.; Yadav, S.; Padaki, M.; Zadorozhnyy, V.; Pai, R.K. Al-Ti₂O₆ a mixed metal oxide based composite membrane: A unique membrane for removal of heavy metals. *Chem. Eng. J.* **2018**, *348*, 678–684. [[CrossRef](#)]
- Fu, F.; Wang, Q. Removal of heavy metal ions from wastewaters: A review. *J. Environ. Manag.* **2011**, *92*, 407–418. [[CrossRef](#)]

6. Manfoudhi, N.; Boufi, S. Porous material from cellulose nanofibrils coated with aluminum hydroxyde as an effective adsorbent for fluoride. *J. Environ. Chem. Eng.* **2020**, *8*, 103779. [[CrossRef](#)]
7. Manfoudhi, N.; Boufi, S. Nanocellulose as a novel nanostructured adsorbent for environmental remediation: A review. *Cellulose* **2017**, *24*, 1171–1197. [[CrossRef](#)]
8. Chen, Q.; Zheng, J.; Wen, L.; Yang, C.; Zhang, L. A multi-functional-group modified cellulose for enhanced heavy metal cadmium adsorption: Performance and quantum chemical mechanism. *Chemosphere* **2019**, *224*, 509–518. [[CrossRef](#)]
9. Rani, K.; Gomathi, T.; Vijayalakshmi, K.; Saranya, M.; Sudha, P.N. Banana fiber cellulose nano crystals grafted with butyl acrylate for heavy metal lead (II) removal. *Int. J. Biol. Macromol.* **2019**, *131*, 461–472.
10. Kardam, A.; Raj, K.R.; Srivastava, S.; Srivastava, M.M. Nanocellulose fibers for biosorption of cadmium, nickel, and lead ions from aqueous solution. *Clean. Technol. Environ. Policy* **2013**, *16*, 385–393. [[CrossRef](#)]
11. Qu, J.; Tian, X.; Jiang, Z.; Cao, B.; Akindolie, M.S.; Hu, Q.; Feng, C.; Feng, Y.; Meng, X.; Zhang, Y. Multi-component adsorption of Pb(II), Cd(II) and Ni(II) onto microwave-functionalized cellulose: Kinetics, isotherms, thermodynamics, mechanisms and application for electroplating wastewater purification. *J. Hazard. Mater.* **2020**, *387*, 121718. [[CrossRef](#)]
12. Zhang, Y.; Yue, X.; Xu, W.; Zhang, H.; Li, F. Amino modification of rice straw-derived biochar for enhancing its cadmium (II) ions adsorption from water. *J. Hazard. Mater.* **2019**, *379*, 120783. [[CrossRef](#)]
13. Puangsin, B.; Fujisawa, S.; Kuramae, R.; Saito, T.; Isogai, A. TEMPO-mediated oxidation of hemp bast holocellulose to prepare cellulose nanofibrils dispersed in water. *J. Polym. Environ.* **2013**, *21*, 555–563. [[CrossRef](#)]
14. Kuramae, R.; Saito, T.; Isogai, A. TEMPO-oxidized cellulose nanofibrils prepared from various plant holocelluloses. *React. Funct. Polym.* **2014**, *85*, 126–133. [[CrossRef](#)]
15. Saito, T.; Isogai, A. TEMPO-mediated oxidation of native cellulose. The effect of oxidation conditions on chemical and crystal structures of the water-insoluble fractions. *Biomacromolecules* **2004**, *5*, 1983–1989. [[CrossRef](#)]
16. Khanjani, P.; Kosonen, H.; Ristolainen, M.; Virtanen, P.; Vuorinen, T. Interaction of divalent cations with carboxylate group in TEMPO-oxidized microfibrillated cellulose systems. *Cellulose* **2019**, *26*, 4841–4851. [[CrossRef](#)]
17. Cao, L.; Li, Z.; Xiang, S.; Huang, Z.; Ruan, R.; Liu, Y. Preparation and characteristics of bentonite–zeolite adsorbent and its application in swine wastewater. *Bioresour. Technol.* **2019**, *284*, 448–455. [[CrossRef](#)]
18. Kostenko, L.; Artiushenko, O.; Kovalchuk, T.; Tomashchuk, I.; Zaitsev, V. Preparation and characterization of organofunctionalized bentonite clay bearing aminophosphonic groups in heavy metal uptake. *J. Environ. Chem. Eng.* **2019**, *7*, 103434. [[CrossRef](#)]
19. Ain, Q.U.; Rasheed, U.; Yaseen, M.; Zhang, H.; Tong, Z. Superior dye degradation and adsorption capability of polydopamine modified Fe₃O₄-pillared bentonite composite. *J. Hazard. Mater.* **2020**, *397*, 122758. [[CrossRef](#)]
20. Khandal, D.; Riedl, B.; Tavares, J.R.; Carreau, P.J.; Heuzey, M.-C. Tailoring cellulose nanocrystals rheological behavior in aqueous suspensions through surface functionalization with polyethyleneimine. *Phys. Fluids* **2019**, *31*, 021207. [[CrossRef](#)]
21. Song, L.; Liu, F.; Zhu, C.; Li, A. Facile one-step fabrication of carboxymethyl cellulose based hydrogel for highly efficient removal of Cr(VI) under mild acidic condition. *Chem. Eng. J.* **2019**, *369*, 641–651. [[CrossRef](#)]
22. Qin, F.; Fang, Z.; Zhou, J.; Sun, C.; Chen, K.; Ding, Z.; Li, G.; Qiu, X. Efficient removal of Cu²⁺ in water by carboxymethylated cellulose nanofibrils: Performance and mechanism. *Biomacromolecules* **2019**, *20*, 4466–4475. [[CrossRef](#)] [[PubMed](#)]
23. Jin, X.; Xiang, Z.; Liu, Q.; Chen, Y.; Lu, F. Polyethyleneimine-bacterial cellulose bioadsorbent for effective removal of copper and lead ions from aqueous solution. *Bioresour. Technol.* **2017**, *244*, 844–849. [[CrossRef](#)] [[PubMed](#)]
24. Hoang, M.T.; Pham, T.D.; Verheyen, D.; Nguyen, M.K.; Pham, T.T.; Zhu, J.; der Bruggen, B.V. Fabrication of thin film nanocomposite nanofiltration membrane incorporated with cellulose nanocrystals for removal of Cu(II) and Pb(II). *Chem. Eng. Sci.* **2020**, *228*, 115998. [[CrossRef](#)]
25. Hong, H.J.; Yu, H.; Park, M.; Jeong, H.S. Recovery of platinum from waste effluent using polyethyleneimine-modified nanocelluloses: Effects of the cellulose source and type. *Carbohydr. Polym.* **2019**, *210*, 167–174. [[CrossRef](#)]
26. Saito, T.; Kimura, S.; Nishiyama, Y.; Isogai, A. Cellulose nanofibers prepared by TEMPO-mediated oxidation of native cellulose. *Biomacromolecules* **2007**, *8*, 2485–2491. [[CrossRef](#)]
27. Saito, T.; Yanagisawa, M.; Isogai, A. TEMPO-mediated oxidation of native cellulose: SEC–MALLS analysis of water-soluble and insoluble fractions in the oxidized products. *Cellulose* **2005**, *12*, 305–315. [[CrossRef](#)]
28. Zhang, N.; Zang, G.-L.; Shi, C.; Yu, H.-Q.; Sheng, G.-P. A novel adsorbent TEMPO-mediated oxidized cellulose nanofibrils modified with PEI: Preparation, characterization, and application for Cu(II) removal. *J. Hazard. Mater.* **2016**, *316*, 11–18. [[CrossRef](#)]
29. Palani, S.; Lingam, R.; Srinivasan, G.R. Synthesis and characterisation of carboxymethyl cellulose based bentonite polymer blend. *Int. J. Recent Technol. Eng.* **2020**, *8*, 5661–5664. [[CrossRef](#)]
30. Luo, H.; Feng, F.; Yao, F.; Zhu, Y.; Yang, Z.; Wan, Y. Improved removal of toxic metal ions by incorporating graphene oxide into bacterial cellulose. *J. Nanosci. Nanotechnol.* **2020**, *20*, 719–730. [[CrossRef](#)]
31. Liu, M.; Liu, Y.; Shen, J.; Zhang, S.; Liu, X.; Chen, X.; Ma, Y.; Ren, S.; Fang, G.; Li, S.; et al. Simultaneous removal of Pb²⁺, Cu²⁺ and Cd²⁺ ions from wastewater using hierarchical porous polyacrylic acid grafted with lignin. *J. Hazard. Mater.* **2020**, *392*, 122208. [[CrossRef](#)]
32. dos Reis, G.S.; Sampaio, C.H.; Lima, E.C.; Wilhelm, M. Preparation of novel adsorbents based on combinations of polysiloxanes and sewage sludge to remove pharmaceuticals from aqueous solutions. *Colloids Surf. A Physicochem. Eng. Asp.* **2016**, *497*, 304–315. [[CrossRef](#)]
33. Agaba, A.; Cheng, H.; Zhao, J.; Zhang, C.; Tebyetekerwa, M.; Rong, L.; Sui, X.; Wang, B. Precipitated silica agglomerates reinforced with cellulose nanofibrils as adsorbents for heavy metals. *RSC Adv.* **2018**, *8*, 33129–33137. [[CrossRef](#)]

34. Sun, Y.; Liu, X.; Lv, X.; Wang, T.; Xue, B. Synthesis of novel lignosulfonate-modified graphene hydrogel for ultrahigh adsorption capacity of Cr(VI) from wastewater. *J. Clean. Prod.* **2021**, *295*, 126406. [[CrossRef](#)]
35. Pottathara, Y.B.; Narwade, V.N.; Bogle, K.A.; Kokol, V. TEMPO-oxidized cellulose nanofibrils–graphene oxide composite films with improved dye adsorption properties. *Polym. Bull.* **2020**, *77*, 6175–6189. [[CrossRef](#)]
36. Dai, H.; Huang, Y.; Huang, H. Eco-friendly polyvinyl alcohol/carboxymethyl cellulose hydrogels reinforced with graphene oxide and bentonite for enhanced adsorption of methylene blue. *Carbohydr. Polym.* **2018**, *185*, 1–11. [[CrossRef](#)]
37. Hokkanen, S.; Doshi, B.; Srivastava, V.; Puro, L.; Koivula, R. Arsenic (III) removal from water by hydroxyapatite-bentonite clay-nanocrystalline cellulose. *Environ. Progr. Sustain. Energy* **2019**, *38*, 13147. [[CrossRef](#)]
38. Gopinath, S.; Sugunan, S. Enzymes immobilized on montmorillonite K 10: Effect of adsorption and grafting on the surface properties and the enzyme activity. *Appl. Clay Sci.* **2007**, *35*, 67–75. [[CrossRef](#)]
39. Ahmad, R.; Hasan, I. L-cystein modified bentonite-cellulose nanocomposite (cellu/cys-bent) for adsorption of Cu²⁺, Pb²⁺, and Cd²⁺ ions from aqueous solution. *Sep. Sci. Technol.* **2016**, *51*, 381–394. [[CrossRef](#)]
40. Liu, D.; Bian, Q.; Li, Y.; Wang, Y.; Xiang, A.; Tian, H. Effect of oxidation degrees of graphene oxide on the structure and properties of poly (vinyl alcohol) composite films. *Compos. Sci. Technol.* **2016**, *129*, 146–152. [[CrossRef](#)]
41. Qin, L.; Yan, L.; Chen, J.; Liu, T.; Yu, H.; Du, B. Enhanced removal of Pb²⁺, Cu²⁺, and Cd²⁺ by amino-functionalized magnetite kaolin clay. *Ind. Eng. Chem. Res.* **2016**, *55*, 7344–7354. [[CrossRef](#)]
42. Larraza, I.; López-González, M.; Corrales, T.; Marcelo, G. Hybrid materials: Magnetite–Polyethylenimine–Montmorillonite, as magnetic adsorbents for Cr(VI) water treatment. *J. Colloid Interf. Sci.* **2012**, *385*, 24–33. [[CrossRef](#)] [[PubMed](#)]
43. Chen, H.; Li, Y.; Wang, S.; Zhou, Y. Synthesis of montmorillonite/Fe₃O₄-OTAB composite capable of using as anisotropic nanoparticles. *Appl. Surf. Sci.* **2017**, *402*, 384–391. [[CrossRef](#)]
44. Chen, X.; Cui, J.; Xu, X.; Sun, B.; Zhang, L.; Dong, W.; Chen, C.; Sun, D. Bacterial cellulose/attapulgitic magnetic composites as an efficient adsorbent for heavy metal ions and dye treatment. *Carbohydr. Polym.* **2019**, *229*, 115512. [[CrossRef](#)]
45. Lu, B.; Lin, Q.; Yin, Z.; Lin, F.; Chen, X.; Huang, B. Robust and lightweight biofoam based on cellulose nanofibrils for high-efficient methylene blue adsorption. *Cellulose* **2021**, *28*, 273–288. [[CrossRef](#)]
46. Yu, X.; Tong, S.; Ge, M.; Zuo, J.; Cao, C.; Song, W. One-step synthesis of magnetic composites of cellulose@iron oxide nanoparticles for arsenic removal. *J. Mater. Chem. A* **2013**, *1*, 959–965. [[CrossRef](#)]
47. Jiang, R.; Zhu, H.Y.; Fu, Y.Q.; Zong, E.M.; Jiang, S.T.; Li, J.B.; Zhu, J.Q.; Zhu, Y.Y. Magnetic NiFe₂O₄/MWCNTs functionalized cellulose bioadsorbent with enhanced adsorption property and rapid separation. *Carbohydr. Polym.* **2021**, *252*, 117158. [[CrossRef](#)]
48. Xing, X.; Li, W.; Zhang, J.; Wu, H.; Guan, Y.; Gao, H. TEMPO-oxidized cellulose hydrogel for efficient adsorption of Cu²⁺ and Pb²⁺ modified by polyethyleneimine. *Cellulose* **2021**, *28*, 7953–7968. [[CrossRef](#)]
49. Chen, Q.; Zheng, J.; Zheng, L.; Dang, Z.; Zhang, L. Classical theory and electron-scale view of exceptional Cd(II) adsorption onto mesoporous cellulose biochar via experimental analysis coupled with DFT calculations. *Chem. Eng. J.* **2018**, *350*, 1000–1009. [[CrossRef](#)]
50. Park, S.H.; Shin, S.S.; Park, C.H.; Jeon, S.; Gwon, J.; Lee, S.Y.; Kim, S.J.; Kim, H.J.; Lee, J.H. Poly(acryloyl hydrazide)-grafted cellulose nanocrystal adsorbents with an excellent Cr(VI) adsorption capacity. *J. Hazard. Mater.* **2020**, *394*, 122512. [[CrossRef](#)]
51. Mahdavinia, G.R.; Soleymani, M.; Sabzi, M.; Azimi, H.; Atlasi, Z. Novel magnetic polyvinyl alcohol/laponite RD nanocomposite hydrogels for efficient removal of methylene blue. *J. Environ. Chem. Eng.* **2017**, *5*, 2617–2630. [[CrossRef](#)]
52. Wang, Z.; Zhou, W.; Zhu, L. Mono-/competitive adsorption of cadmium(II) and lead(II) using straw/bentonite-g-poly(acrylic acid-co-acrylamide) resin. *Polym. Bull.* **2019**, *77*, 3795–3811. [[CrossRef](#)]
53. Das, S.; Das, P.; Chakraborty, S. Optimization of hazardous crystal violet by chemically treated rice husk: Using central composite response surface methodology. *Arch. Environ. Sci.* **2012**, *6*, 57–61.
54. Chakraborty, S.; Chowdhury, S.; Saha, P.D. Adsorption of crystal violet from aqueous solution onto NaOH-modified rice husk. *Carbohydr. Polym.* **2011**, *86*, 1533–1541. [[CrossRef](#)]
55. Chakraborty, S.; Mukherjee, A.; Das, S.; Maddela, N.R.; Iram, S.; Das, P. Study on isotherm, kinetics, and thermodynamics of adsorption of crystal violet dye by calcium oxide modified fly ash. *Environ. Eng. Res.* **2020**, *26*, 190372. [[CrossRef](#)]
56. Hokkanen, S.; Bhatnagar, A.; Srivastava, V.; Suorsa, V.; Sillanpää, M. Removal of Cd²⁺, Ni²⁺ and PO₄³⁻ from aqueous solution by hydroxyapatite-bentonite clay-nanocellulose composite. *Int. J. Biol. Macromol.* **2018**, *118*, 903–912. [[CrossRef](#)]
57. Liu, S.; Xie, Z.; Zhu, Y.; Zhu, Y.; Jiang, Y.; Wang, Y.; Gao, H. Adsorption characteristics of modified rice straw biochar for Zn and in-situ remediation of Zn contaminated soil. *Environ. Technol. Innov.* **2021**, *22*, 101388. [[CrossRef](#)]
58. Adil, H.I.; Thalji, M.R.; Yasin, S.A.; Saeed, I.A.; Assiri, M.A.; Chong, K.F.; Ali, G.A.M. Metal–organic frameworks (MOFs) based nanofiber architectures for the removal of heavy metal ions. *RSC Adv.* **2022**, *12*, 1433–1450. [[CrossRef](#)]
59. Shayegan, H.; Ali, G.A.M.; Safarifard, V. Recent progress in the removal of heavy metal ions from water using metal-organic frameworks. *ChemistrySelect* **2020**, *5*, 124–146. [[CrossRef](#)]
60. Shayegan, H.; Ali, G.A.M.; Safarifard, V. Amide-functionalized metal–organic framework for high efficiency and fast removal of Pb (II) from aqueous solution. *J. Inorg. Organomet. Polym. Mater.* **2020**, *30*, 3170–3178. [[CrossRef](#)]
61. Sadegh, H.; Ali, G.A.M.; Makhlof, A.S.H.; Chong, K.F.; Alharbi, N.S.; Agarwal, S.; Gupta, V.K. MWCNTs-Fe₃O₄ nanocomposite for Hg(II) high adsorption efficiency. *J. Mol. Liq.* **2018**, *258*, 345–353. [[CrossRef](#)]